Soils and Foundations 63 (2023) 101301 https://doi.org/10.1016/j.sandf.2023.101301

Effect of temperature on the soil–water retention characteristics in unsaturated soils: Analytical and experimental approaches

Tuan A. Pham, Amirhossein Hashemi, Melis Sutman, Gabriela M. Medero

[Outline]

Temperature effect on soil-water retention curve (SWRC)

Develops a new predictive model to estimate SWRC at different temperatures{thermo-hydro-mechanical behavior of soils}

[Methods]

Reviewed the constitutive laws governing the thermal-hydro-mechanical (THM) behavior – suction with w, t, e.

Model considers the effects of surface tension, contact angle, D, e, and ρ_w on matric suction.

[Results]

SWRC decreases significantly as temperature increases.

At 24°C, matric suction is reduced by 26% when 45°C.

Analytical model demonstrated good performance in predicting the SWRC under non-isothermal conditions, outperforming existing models in terms of accuracy.

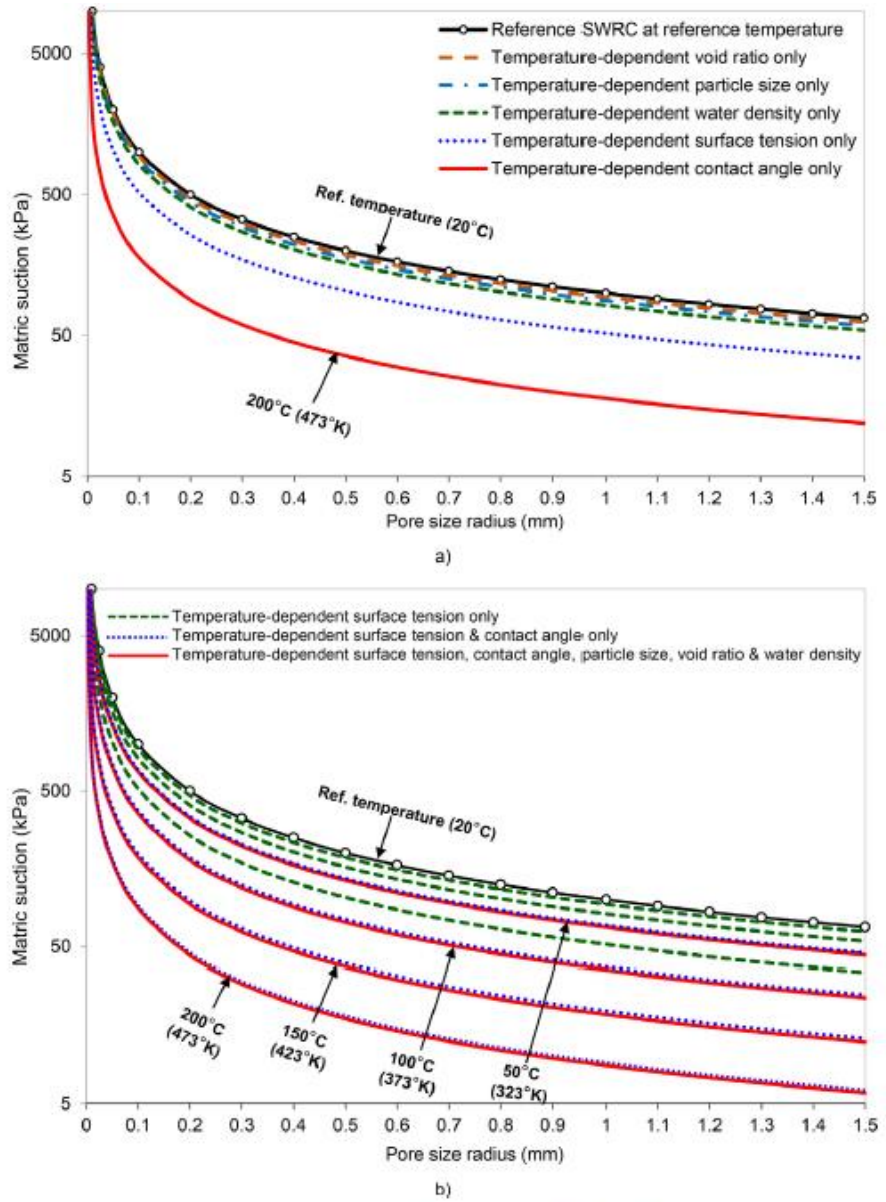

Fig. 2. Matric suction versus pore size for: a) considering different functions at 200 °C, and b) considering various range of temperature.

Soils and Foundations 63 (2023) 101313 https://doi.org/10.1016/j.sandf.2023.101313

Evaluating barrier performance of geomembranes against 1,4-dioxane and bisphenol a in landfill leachates

Hiroyuki Ishimori, Kazuto Endo, Tomonori Ishigaki, Masato Yamada

[Outline]
Assess barrier performance of geomembranes against 1,4-dioxane and bisphenol A in landfill leachates, which are hazardous pollutants, New insights into the effectiveness of various geomembranes (PVC, LDPE, HDPE) in preventing permeation of these pollutants

[Methods]
Diffusive permeation tests using four types of geomembranes: 0.5 mm PVC, 1.5 mm PVC, 1.5 mm LDPE, and 1.5 mm HDPE. Benzene, bisphenol A, and 1,4-dioxane to measure the permeation rates through these geomembranes.
Mathematical model used for evaluating partitioning and diffusion coefficients was fitted to the experimental data using the least-squares method.

[Results]
Partitioning coefficient (K) and diffusion coefficient (D) were determined for each geomembrane and pollutant combination.
Relative concentration of benzene converged to about 0.2 in PVC, indicating high absorbability, while HDPE showed longer permeation times, indicating better barrier performance.
Bisphenol A showed a high absorbability with source concentrations around 0.45, suggesting it did not leach significantly from the geomembranes during the test.

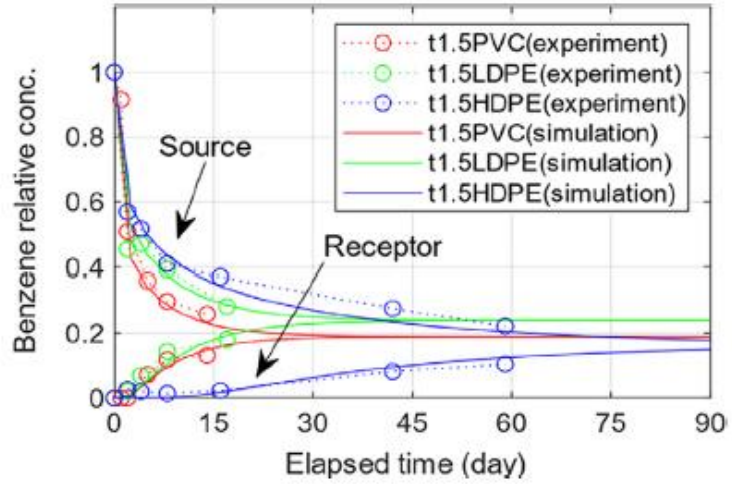

Fig. 2. Concentrations of benzene permeating in and leaching out of 1.5-mm-thick geomembranes.

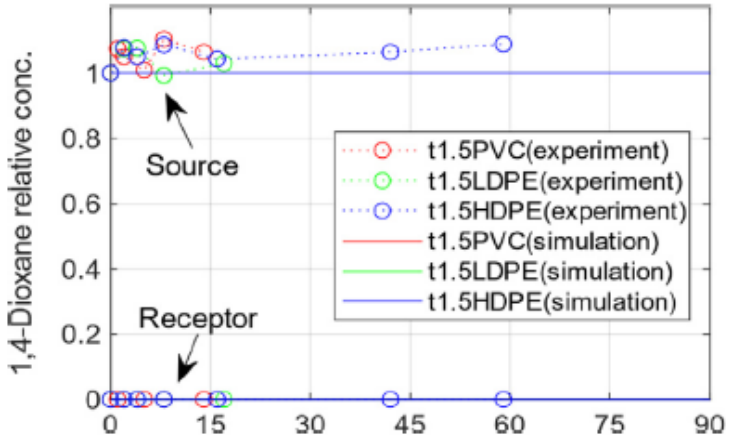

Fig. 4. Concentrations of 1,4-dioxane permeating in and leaching out of 1.5-mm-thick geomembranes.

Soils and Foundations 63 (2023) 10131 9 https://doi.org/10.1016/j.sandf.2023.101319

Evaluation of natural and artificial fiber reinforcements on the mechanical properties of cement-stabilized dredged sediment

Jiang-Shan Li, Xin Chen, Lei Lang, Xing-Xing He, Qiang Xue

[Outline]

fibers → Improve the mechanical properties of dredged sediment stabilized with cement.

Dredged sediment has poor engineering properties

1. polypropylene fiber (PF)
2. straw fiber (SF) as artificial and natural reinforcements

[Methods]

Target: cement-stabilized dredged sediment (CDS)

Unconfined compressive strength (UCS) tests → cement contents, fiber contents, fiber lengths, and w.

Microstructural analysis; investigate interfacial friction and [bridge] effect between fibers and cemented sediment matrix.

[Results]

max UCS of CDS with PF at 7, 28, 60, and 90 days increased by 17.7%, 43.6%, 10.7%, and 9.7%.

In contrast, the inclusion of SF tended to decrease the UCS.

Optimal PF length was found to be 3 mm, and the optimal SF length was 5-10 mm. Increasing cement content or decreasing water content aggravated brittleness of CPFDS and CSFDS.

Both PF and SF effectively improved the ductility of CDS, with more pronounced ductile behavior observed with increasing fiber content.

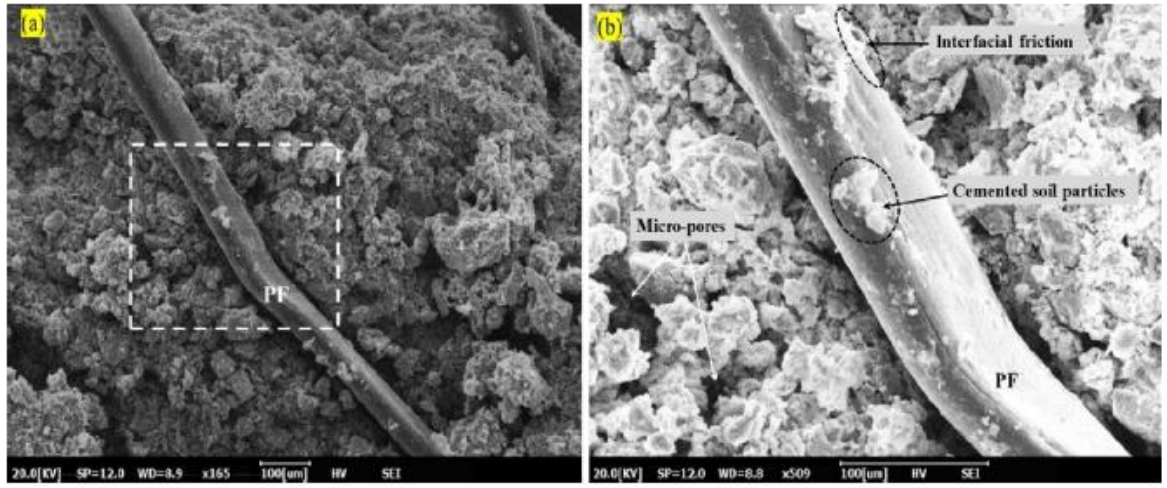

Fig. 17. SEM micrographs of typical 28-day CPFDS with magnification of (a) 165 × and (b) 509×.

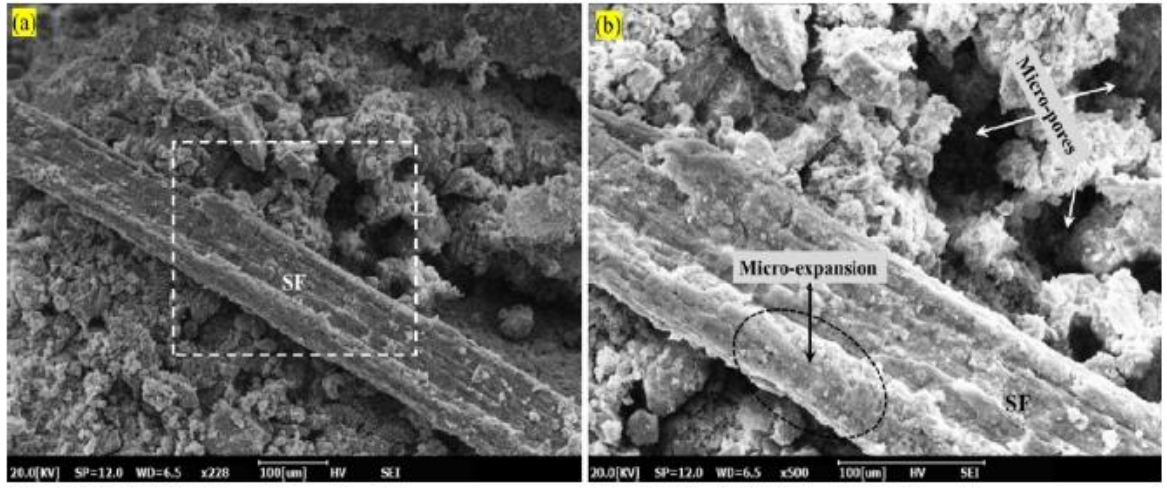

Fig. 18. SEM micrographs of typical 28-day CSFDS with magnification of (a) 228 × and (b) 500×.

Soils and Foundations 63 (2023) 101324 https://doi.org/10.1016/j.sandf.2023.101324

Experimental study of the interface evolution behavior and softening mechanism of structure-marine soil

Qing Yang, Zheng Zheng, M. Hesham El Naggar, Gangqiang Kong, Shixing Zhang, Gang Yang, Yubin Ren

[Outline]

Designing offshore platforms due to the undrained interface characteristics of marine clay-structures

New interface instrument that facilitates the accurate evaluation of interfacial shear-induced pore pressure, aiding in understanding the undrained interfacial behavior and strain softening mechanisms.

[Methods]

Newly developed interface instrument based on a static/dynamic hydraulic triaxial shear device to measure interface shear-induced EPWP accurately.

The device was employed to conduct undrained interface tests on marine soils with different initial moisture contents, focusing on macroscopic mechanical behavior and microscopic interfacial particle migration

[Results]

Peak shear strength for soils with initial w of 81% decreased from 0.264 to 0.216 as the confining pressure increased from 50~200 kPa. For soils with of 76%, 81%, 86%, the interfacial shear-induced pore pressure increased with higher and higher, indicating a thicker water film at the interface.

Effective ϕ remained almost constant, while effective adhesion decreased by 25.3% as increased, showing that w primarily affected interface adhesion.

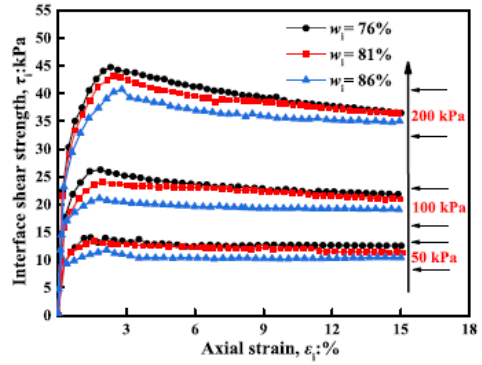

Fig. 6. Stress–strain curves at the undrained interface under different initial moisture contents: 76%, 81% and 86%.

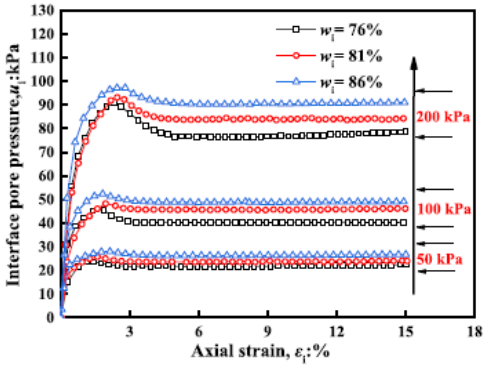

Fig. 8. Variation in the interfacial shear-induced excess pore pressure u_i with strain ε_i for specimens with different initial moisture contents.

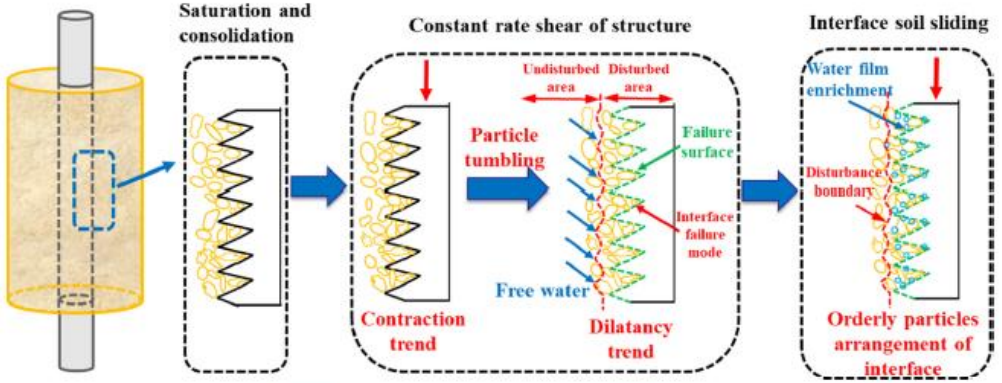

Fig. 19. Microevolution processes of the soil surrounding the interface.

Soils and Foundations 63 (2023) 101326 https://doi.org/10.1016/j.sandf.2023.101326

Experimental study on sand anisotropy using hollow cylinder apparatus

Shotaro Yamada, Maki Okada, Masaki Nakano, Toshihiro Noda

[Outline]

Effect of sand anisotropy on shear behavior

New insights by systematically investigating the initial and induced anisotropy in sand using a hollow cylinder apparatus (HCA).

[Methods]

HCA to investigate the anisotropic behavior of Toyoura sand.

Undrained shear tests under different principal stress directions and intermediate principal stresses.

[Results]

Peak shear strength of sand decreased with increase in the intermediate principal stress factor (β), and failure angle (αf) increased as β increased, aligning well with Lade-Duncan failure criterion.

Undrained shear strength of sand with an initial Dr of 60% varied depending on the direction of shear, with specimens exhibiting pseudo-density changes and behaving similarly to loose or dense sand based on the anisotropic direction.

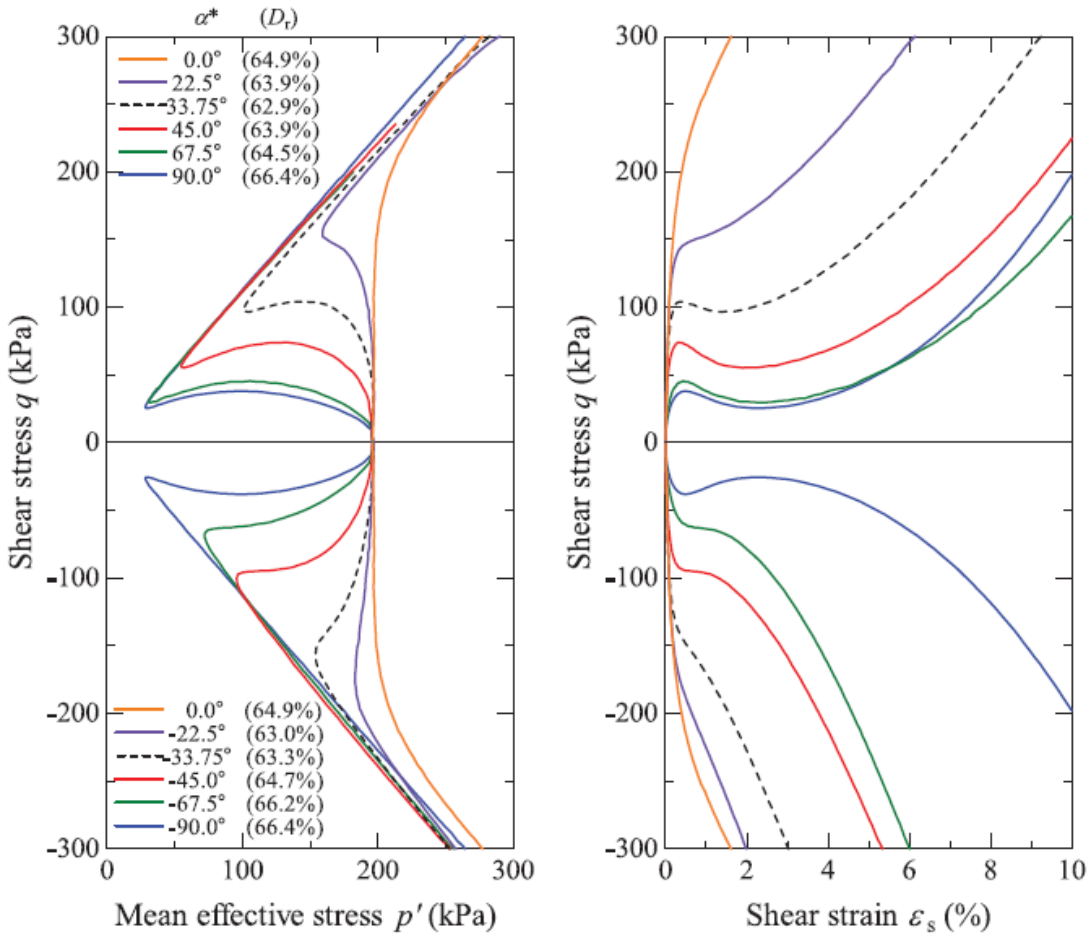

Fig. 19. Undrained shear test results with different principal stress directions for specimens subjected to same prior shear history as in Fig. 15 (c) (sample preparation: air deposition method). * Data are reorganized using a *.

Soils and Foundations 63 (2023) 101300 https://doi.org/10.1016/j.sandf.2023.101300

Extraction of crude soybean urease using ethanol and its effect on soil cementation

Han-Jiang Lai, Ming-Juan Cui, Shi-Fan Wu, Yang Yang, Jian Chu

[Outline]

Effectiveness of using ethanol in extraction of urease from soybeans.

Novel approach to producing a more effective crude urease solution for use in Enzyme Induced Carbonate Precipitation (EICP) treatments

[Methods]

Grinding-extraction method to obtain crude soybean urease, involving mixing of soybean powder with distilled water containing various ethanol contents (EC). The urease activity and turbidity of extracted solutions were measured to evaluate effectiveness of different ethanol concentrations. Sand columns were prepared and treated with crude urease solutions, followed by tests to assess calcium carbonate precipitation and unconfined compressive strength.

[Results]

Urease activity of the extracted enzyme solution decreased with increasing ethanol content, with the optimal range found to be 20%-30% (v/v) for preparing a 100 g/L crude soybean urease solution. The crude urease solution extracted with higher ethanol content (EC) showed reduced turbidity and more uniform calcium carbonate distribution in the treated sand columns. The unconfined compressive strength (quc) of the cemented sand columns was highest when treated with urease solutions.

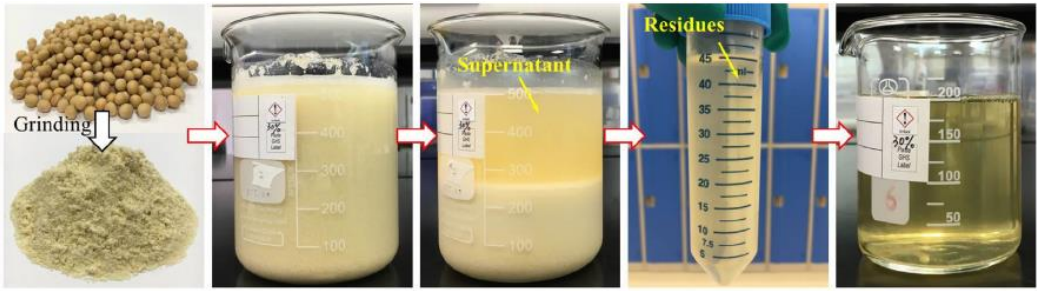

(a) Grinding the dry soybean into powder | (b) Mixing soybean powder with distilled water containing ethanol and stirring for 30 min | (c) Settling the mixed solution in 4°C refrigerator for 12 h | (d) Centrifuging the supernatant at 4°C with 10000 rpm for 15 min | (e) Collecting crude soybean urease solution

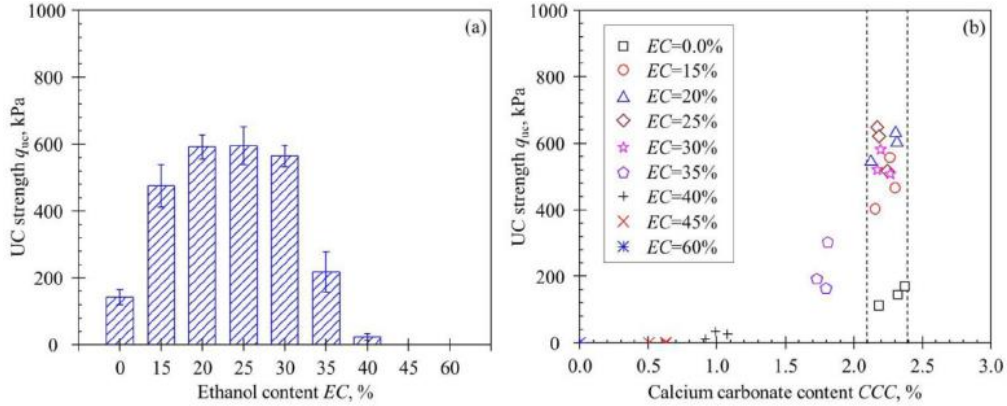

Fig. 8. UC strength q_{uc} of cemented sand column: (a) q_{uc} versus *EC*; and (b) q_{uc} versus *CCC*.

Soils and Foundations 63 (2023) 101311 https://doi.org/10.1016/j.sandf.2023.101311

Failure envelope considering the ultimate tensile capacity of suction caissons in sand

Hiroyoshi Hirai

[Outline]

Impact of ultimate tensile capacity on failure envelope of soils

New method to incorporate tensile strength into analysis of soil behavior under different loading conditions.

[Methods]

Series of laboratory tests to measure the tensile strength of different soil samples.

Various loading scenarios and capture the soil's response, particularly focusing on its tensile capacity.

Advanced computational models were then developed to integrate these experimental results, allowing for a detailed analysis of how tensile strength affects the overall failure envelope.

[Results]

Incorporating tensile capacity significantly alters the failure envelope of soils.

Inclusion of ultimate tensile strength increased the predicted failure stress by approximately 15% under certain loading conditions.

Soils with higher tensile strength exhibited greater resistance to deformation, with a measured tensile capacity ranging from 50 kPa to 150 kPa across different samples.

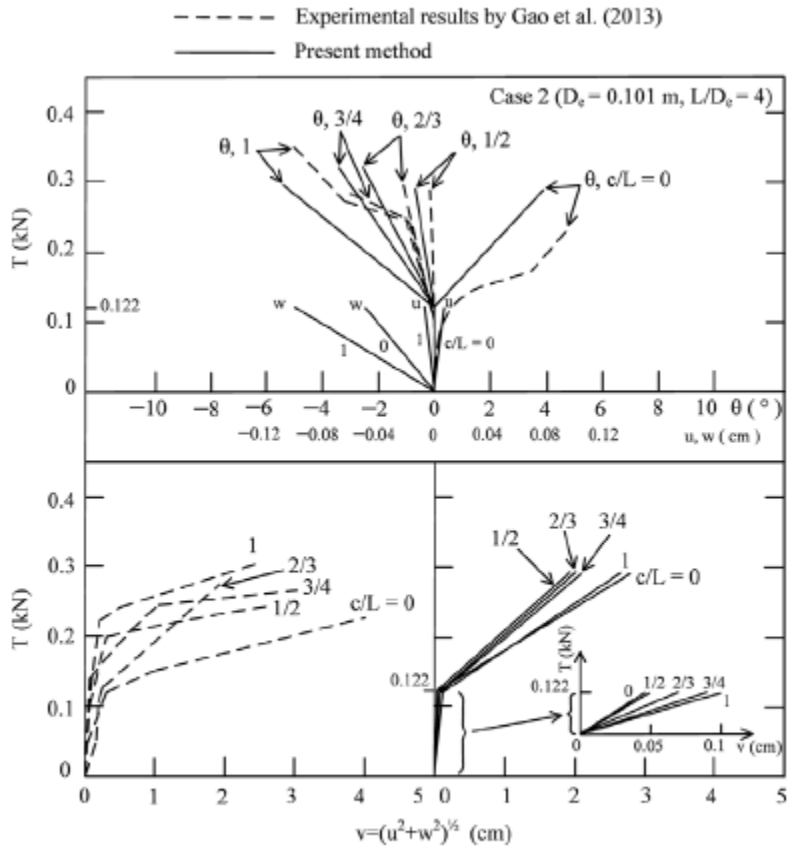

Fig. 7. Displacement and rotation produced by inclined tensile load for suction caisson in Case 2 in medium dense sand when ω = 60°.